Available online at www.sciencedirect.com

ScienceDirect

Optics & Laser Technology 40 (2008) 941–945

Optics & Laser Technology

www.elsevier.com/locate/optlastec

Structure and optical damage resistance of near-stoichiometric Zn:Fe:LiNbO$_3$ crystals

Fu Ri Ling[a,*], Zhi Hong He[b], Jian Quan Yao[a], Baio Wang[b], Shao Ji Jiang[b]

[a] *Wuhan National Laboratory for Optoelectronics, School of Optoelectronics Science and Engineering, Huazhong University of Science and Technology, Wuhan 430074, PR China*

[b] *Institute of Optoelectronic and Composite Materials, School of Physics and Engineering, Sun Yat-sen University, Guangzhou 510275, PR China*

Received 19 May 2007; received in revised form 26 December 2007; accepted 2 January 2008
Available online 21 February 2008

Abstract

A series of near-stoichiometric Zn:Fe:LiNbO$_3$ crystals were grown by the high-temperature top-seed solution growth (HTTSSG) method from stoichiometric melts doped with 6 mol% K$_2$O. Infrared (IR) transmission spectra were measured and discussed in terms of the defect structure of the near-stoichiometric Zn:Fe:LiNbO$_3$ crystals. The results of the transmitted beam pattern distortion method show that the optical damage resistance of the near-stoichiometric Zn:Fe:LiNbO$_3$ crystals increases rapidly when the ZnO concentration exceeds a threshold value. The threshold value concentration of ZnO of the near-stoichiometric Zn:Fe:LiNbO$_3$ crystals is much lower than that of the congruent LiNbO$_3$ crystals. The dependence of the optical damage resistance on the defect structure of the near-stoichiometric Zn:Fe:LiNbO$_3$ crystals are discussed, and the holographic recording properties of the near-stoichiometric Zn:Fe:LiNbO$_3$ crystals are investigated.

Keywords: Stoichiometric; Optical damage resistance; Zn:Fe:LiNbO$_3$ crystals

1. Introduction

The LiNbO$_3$ is one of the most widely used electro-optical materials. Its excellent photorefractive properties mean that the most important application is holographic storage. Almost all commercially available LiNbO$_3$ crystals are typical non-stoichiometric compositions, which are grown from a congruent composition melt ([Li]/[Nb] = 0.946, atomic ratio) [1]. Although congruent LiNbO$_3$ (CLN) crystals generally have good quality and uniformity, near-stoichiometric LiNbO$_3$ (SLN) crystals are thought to be superior, with fewer defects because of the increased Li content in the crystal lattice. Thus, the improvement of the optical properties in SLN crystals, such as shorter response time [2], higher exponential gain coefficient [3], higher sensitivity and dynamic range [4], stronger photo-damage resistance ability [5–7], large electro-ferroelectric [8], and shorter absorption edge [9], compared with those of CLN crystals, have been reported.

On the other hand, it is well known that the applications of LiNbO$_3$ are severely limited by optical damage, which induces a birefringence change at high laser intensities [10,11]. Although some methods have been proposed to improve the signal-to-noise ratio [12,13], the best way to solve this problem is to optimize the crystal itself. Doping with damage-resistant dopants is found to be an effective method to increase the optical damage resistance [14]. Some damage-resistant elements, such as Mg [15], Zn [16], In [17,18], and Sc [19], have been used to decrease the optical damage of the LiNbO$_3$ crystals. Recently, Zhang et al. reported that an LiNbO$_3$ crystal with 6.0 mol% ZnO exhibited an excellent optical damage-resistance property due to the ZnO concentration exceeding a threshold value [20].

In this paper, a series of Zn:Fe:SLN crystals were grown, doped with a range of ZnO concentrations, to enhance the optical damage resistance. The dependence of optical damage resistance on the structure defects is discussed.

---

*Corresponding author. Fax: +86 20 84110530.
E-mail address: lingfuri@mail.sysu.edu.cn (F.R. Ling).

0030-3992/$ - see front matter © 2008 Published by Elsevier Ltd.
doi:10.1016/j.optlastec.2008.01.012

Infrared (IR) transmission spectra were measured to investigate the structure of the crystals and at the same time holographic storage was characterized to investigate the recording properties of the crystals.

2. Experiment

2.1. Crystal preparation

The near-SLN crystals were grown by the HTTSSG method from K_2O–Li_2O–Nb_2O_5 fluxes [21–23] using a medium-frequency induction heater furnace. The growth was along the *c*-direction with the negative polarization of the seed facing the melt from the polycrystalline material. The raw materials used for crystal growth were K_2CO_3, Li_2CO_3, Nb_2O_5, ZnO, and Fe_2O_3, with a purity of 99.99%. The melt composition for several crystals is shown in Table 1. In order to prepare the doped $LiNbO_3$ polycrystalline materials, the thoroughly mixed raw materials were placed a platinum crucible (70 mm in diameter and 50 mm in height), and calcined at 750 and 1000 °C for 5 h, respectively. The technical conditions of crystal growth are listed in Table 1. For the successful growth of good-quality crystals, a steep thermal gradient above the melt (200–600 °C/cm) was required. The seeding temperature was below the melting temperature of the congruent crystal by more than 150 °C. To keep the composition homogeneity, the crystal growth was abruptly stopped when about 6 wt% of the initial charge had been pulled out, and slowly cooled down to room temperature at a rate of 100 °C/h. All of the crystals were clear and transparent. Test samples were cut from the middle of the crystal and polished to optical-grade smoothness. The size of the samples is listed in Table 1.

2.2. Measurements

An S/max3080E2 style X-ray fluorescence spectroscopic instrument was used to measure the concentration of Zn^{2+} in the Zn:Fe:SLN crystals. The sample powder used in the X-ray fluorescence spectrum measurements was obtained from the top of the Zn:Fe:SLN crystals. The results are shown in Table 1.

The IR transmission spectra of the crystals were obtained with a Fourier IR spectrophotometer in the 3200–3800 cm^{-1} wavenumber range at room temperature.

The transmitted beam pattern distortion method [24] was used to study the optical damage resistance of the doped SLN crystals. Fig. 1 shows the experimental setup. Light from a Ar^+-ion laser (488.0 nm) was focused by means of a convex lens of focal length, *f*, onto a crystal sample placed in the focal plane. The laser beam is polarized parallel to the *c*-axis of the crystal. The diameter of the focused laser beam is related to the incident beam diameter, *d*, determined by the diaphragm, and yields the focused laser beam area given in Eq. (2) for *S*:

$$D = \frac{2f\lambda}{\pi d}, \tag{1}$$

where λ is the wavelength of laser. The focused laser beam area S is obtained as

$$S = \pi\left(\frac{D}{2}\right)^2 = \frac{(f\lambda)^2}{\pi d^2}. \tag{2}$$

When the laser power intensity is low, optical damage is not created in the crystal and the pattern of the transmitted beam on the screen is circular. When the laser intensity exceeds a certain value, optical damage appears within the crystal and the pattern of the transmitted beam is elongated in the direction of the *c*-axis. The critical laser intensity, which induces a distortion of the pattern of the transmitted

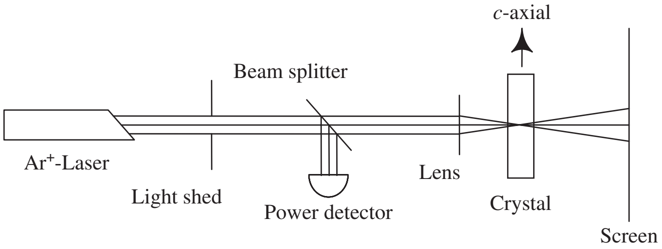

Fig. 1. Experimental setup of the optical damage-resistance measurement.

Table 1
Growth methods and composition of the near Zn:Fe:SLN crystals

	No. 1	No. 2	No. 3	No. 4	No. 5
[ZnO] doping (mol%)	0	0	1	2	3
[Fe_2O_3] doping (ppm)	0	30	30	30	30
[K_2O] doping (mol%)	6	6	6	6	6
[Li]/[Nb] starting composition	1	1	1	1	1
Crystal size (mm^2)	$\phi 30 \times 32$	$\phi 28 \times 30$	$\phi 24 \times 30$	$\phi 20 \times 30$	$\phi 20 \times 30$
Wafer size (mm^3)	10 × 10 × 3	10 × 10 × 3	10 × 10 × 3	10 × 10 × 3	10 × 10 × 3
Growth rate (mm/h)	0.1	0.1	0.1	0.1	0.1
Rotating rate(r/m)	10	12	15	15	18
[ZnO] in crystal (mol)[a]	–	–	0.88	1.64	2.43

[a] It was measured by an X-ray fluorescence analysis.

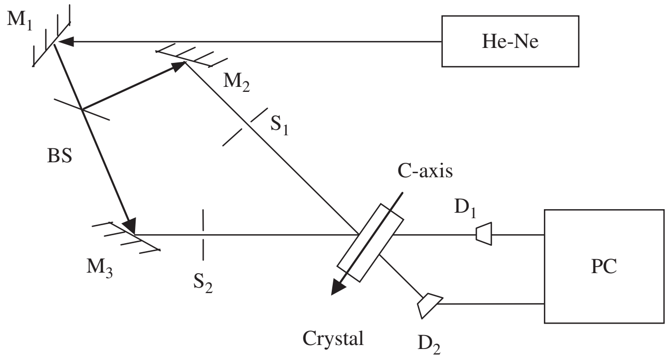

Fig. 2. Experimental light path of holographic storage diffraction efficiency M_1, M_2, M_3: mirrors; BS: beam splitter; D_1,D_2: detector; S_1, S_2: shutters; and PC: computer.

beam, is termed the optical damage resistance (R) of the crystal.

2.3. Holographic recording in the near-Zn:Fe:SLN crystals

Holographic recording was carried out in these crystals at $\lambda = 633\,\mathrm{nm}$. A He–Ne laser ($\lambda = 633\,\mathrm{nm}$) was split into two beams of equal intensity, with each being $20\,\mathrm{mW/cm^2}$. These two beams of extraordinary polarization were made to intersect symmetrically inside the crystal so that the grating vector is parallel to the crystal *c*-axis. In the process of recording, one of the recording beams was blocked by a shutter from time to time, so that we could use the other recording beam to monitor the grating buildup process and to measure the diffraction efficiency η. Here η was defined as $I_d/(I_d+I_t)$, where I_d and I_t were the diffracted and transmitted intensities of the readout beam, respectively. A few percent of diffraction efficiency could be achieved. The experimental light path is shown in Fig. 2.

3. Results and discussion

The IR transmission spectra of the samples are shown in Fig. 3. Two peaks are observed in the IR spectra of nos. 1, 2, and 3, respectively. One peak locating at about $3466\,\mathrm{cm^{-1}}$ is sharp and strong; the other locating at about $3481\,\mathrm{cm^{-1}}$ is weak. For the Zn:Fe:SLN crystals (nos. 4 and 5) with high ZnO doping concentration, a strong OH^- absorption peak locating at about $3529\,\mathrm{cm^{-1}}$ is observed.

The mechanism of the absorption peak shift is described as follows: In the pure SLN crystal, the number of Li^+ is less than that of Nb^{5+} ($Li/Nb<1$). Thus, some Nb^{5+} occupy the Li sites. Thus, the antisite Nb (Nb_{Li}^{4+}) and Li vacancies appear. H^+ is easily attracted by Li vacancies with negative charge. Thus, the site change of the OH^- absorption peak can reflect the change of the environment around the Li vacancy. In Zn:Fe:SLN, Zn^{2+} and Fe^{3+} replace Nb_{Li}^{4+} and Li^+, respectively, to form Zn_{Li}^{+} and Fe_{Li}^{2+} when the concentration of ZnO is lower than its threshold value. H^+ is far away from Zn_{Li}^{+} and Fe_{Li}^{2+} because they repel each other. So the OH^- absorption peaks of the Zn:Fe:SLN crystals (nos. 2 and 3) do not show obvious change compared with that of the pure SLN crystal (no. 1). When the concentration of the ZnO exceeds its threshold value, Zn^{2+} begins to replace the Nb^{5+} and form $(Zn_{Li})^{+}-(Zn_{Nb})^{3-}$ pairs. H^+ ions aggregate around the Zn_{Nb}^{3-} because of the stronger attraction between $(Zn_{Nb})^{3-}$ and H^+. The oscillation energy needed by OH^- to absorb a photon increases. This causes the OH^- absorption peaks of nos. 4 and 5 to shift to a shorter wavelength ($3529\,\mathrm{cm^{-1}}$). It is considered that the new peak located at about $3529\,\mathrm{cm^{-1}}$ corresponds to the oscillation energy of $(Zn_{Li})^{+}-(Zn_{Nb})^{3-}-(OH_{Li})^{-}$. Fe^{3+} contributes little to the shift of the OH^- absorption peak because of its low concentration.

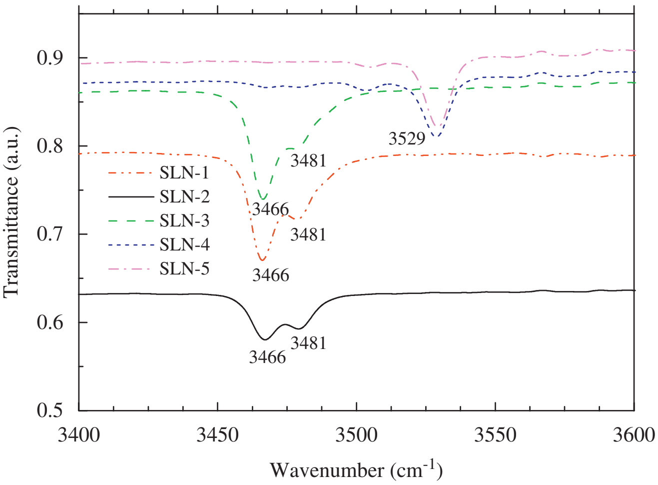

Fig. 3. The IR transmission spectra of the doped near-SLN crystals.

Table 2
The optical damage-resistance ability (R) of the near SLN crystals

Crystal	f (cm)	d (cm)	S (cm^2) $\times 10^{-6}$	I (mW)	R (W/cm^2)
No. 1	5	0.15	1.146	17.48±0.08	$(1.52\pm0.07)\times10^4$
No. 2	5	0.1	3.187	2.12±0.03	$(6.62\pm0.01)\times10^2$
No. 3	5	0.1	3.187	0.45±0.02	$(1.48\pm0.01)\times10^2$
No. 4	5	0.2	0.797	36.51±0.02	$(4.58\pm0.03)\times10^4$
No. 5	5	0.2	0.797	40.34±0.02	$(5.06\pm0.02)\times10^4$

The results of the optical damage-resistance experiment are shown in Table 2 and Fig. 4. The results indicate that the maximum power density that the Zn(2.0 mol%):Fe:SLN crystal (no. 4) and Zn(3.0 mol%):Fe:SLN crystal (no. 5) are able to withstand is up to 4.58×10^4 and $5.06\times10^4\,\mathrm{W/cm^2}$, respectively. It is much higher than that of the pure SLN crystal (no. 1), and is about two orders of magnitude higher than that of both the Fe:SLN (no. 2) and Zn(1.0 mol%):Fe:SLN crystal (no. 3).

Although the reason for the increase of the optical damage resistance is unknown, the following well-known simplified scalar presentation of the photovoltaic field is considered as a possibility. $\partial\Delta n \approx Ak\alpha I/(\sigma_d+\sigma_{ph})$ $(\sigma_d \ll \sigma_{ph})$, where A is the generalized electro-optical coefficient, k the

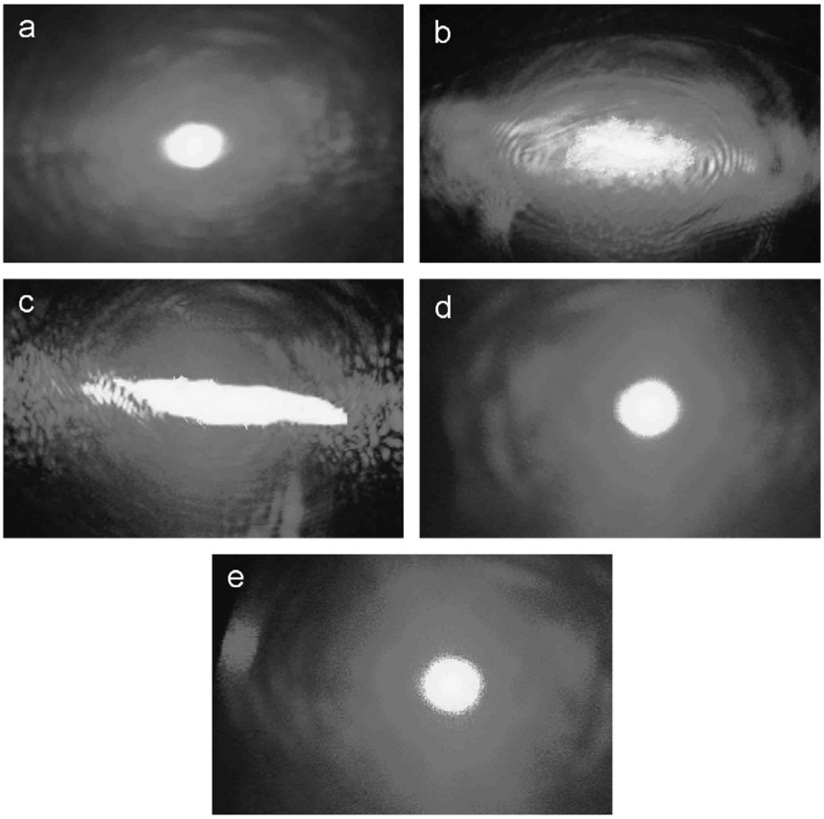

Fig. 4. Distortion of the transmitted Ar^+ ion laser beam spots at steady state (light intensity $5.06 \times 10^4\,W/cm^2$) for the same irradiation times. (a) no. 1; (b) no. 2; (c) no. 3; (d) no. 4; and (e) no. 5.

Glass constant, α the optical absorption coefficient, σ_d the dark conductivity, σ_{ph} the photoconductivity, and I the light intensity [20,25]. With an increase of cation-vacancy photoconductivity, the photorefraction decreases, whereas the photovoltaic current is almost unchanged. If an iron impurity is present, then an abrupt decrease in the capture cross-section of Fe^{3+} acceptors is responsible for the observed increase in σ_{ph} [25]. $[Nb_{Li}^{4+}]$ is the most probable electron acceptor in a Li-deficient $LiNbO_3$ host. Thus, a reduced Nb_{Li} concentration should result in an increase in photoconductivity if the concentration of the concurrent Fe^{3+} acceptor is negligible [26]. In $LiNbO_3$, we may relate an increase of σ_{ph} to a decrease of the Nb_{Li} concentration owing to its replacement by impurities. In SLN crystal, we may attribute the increase of σ_p to the decrease of the Nb_{Li} concentration due to the site of Nb_{Li} being replaced by impurities. But Fe^{3+} substitutes the Li^+ in $Fe:LiNbO_3$. The role of Nb_{Li}^{4+} becomes negligible and σ_p is governed by the electron acceptor Fe^{3+}. So the optical damage resistance of the Fe:SLN (no. 2) is lower than that of the pure near SLN (no. 1). In the Zn:Fe:SLN crystals, the Zn^{2+} substitutes the Nb_{Li}^{4+}, and Fe^{3+} substitutes Li^+. When the concentration of ZnO exceeds a threshold value (under 1.64 mol%), σ_p rapidly increases because Nb_{Li}^{4+} has vanished and most of the Fe ions substitute Nb^{5+}. As such, the optical damage resistance of the Zn:Fe:SLN crystals (nos. 4 and 5) is much higher than that of the $Zn:Fe:LiNbO_3$ (no. 3) crystals with low concentration of ZnO.

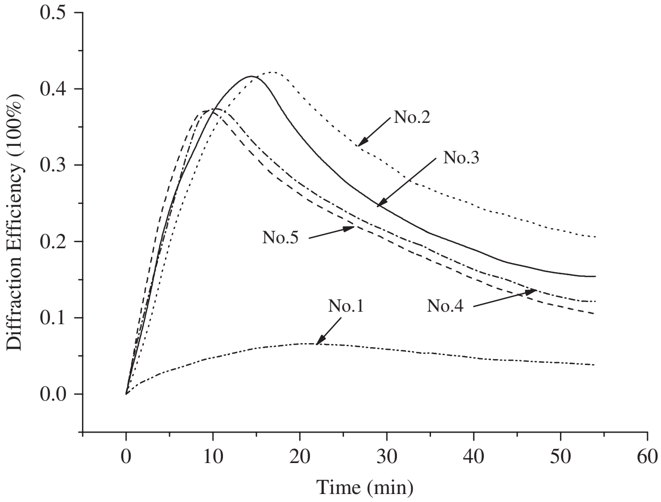

Fig. 5. Recording curves for the doped near-Zn:Fe:SLN crystals.

From Fig. 5, it was found that the recording speed was faster with Zn doping in the crystal, especially with a doping level of Zn(2 mol%), which exceed the so-called threshold concentration. The reason for the difference may be that the doping of Zn increased the photoconductivity of the crystals. This would make the motion of photo-induced charge carriers become faster, and thus would increase the photorefractive response speed. From Fig. 5, it can be seen that there was little change between the recording time of Zn(2 mol%):Fe:$LiNbO_3$ crystal and Zn(3 mol%):Fe:$LiNbO_3$ crystal than the others, which meant that the influence of Zn on the writing times becomes weaker with increasing Zn concentration, which exceed the so-called threshold concentration.

4. Conclusion

Summarizing all of our results, the following conclusions can be made: Zn^{2+} is suggested to preferentially replacing antisite Nb $(Nb_{Li})^{4+}$ defects in Zn:Fe:SLN crystals with Fe^{3+} occupying the Li sites in these crystals. When the concentration of Zn^{2+} exceeds a threshold value (under 1.64 mol%), Nb_{Li}^{4+} vanishes and most of the Fe ions are pushed out from Li sites to substitute Nb^{5+}. The threshold value of the concentration of ZnO in the Zn:Fe:SLN crystal is under 1.64 mol%, which is much lower than that (about 6.0 mol%) in the CLN crystal. The optical damage resistance of the Zn(3.0 mol %):Fe:SLN (no. 5) is observed to be much higher than that of other $LiNbO_3$ crystals.

Acknowledgments

This work was supported by the National Natural Science Fundation of China (10572155), and the Key Industrial Project of Guangdong Province (2005A10602002).

References

[1] Wang HL, Hang Y, Zhang LH, Xu J, He MZ, Zhu SN, et al. J Cryst Growth 2004;262:313.
[2] Chen XJ, Zhu DS, Li B, Ling T, Wu ZK. Opt Lett 2001;26:998.
[3] Chen XJ, Li B, Xu JJ, Zhu DS, Pan SH, Wu ZK. J Appl Phys 2001;90:1516.
[4] Galambos L, Orlov SS, Hessenlink L, Furukawa Y, Kitamura K, Takekawa S. J Cryst Growth 2001;229:228.
[5] Furukawa Y, Kitamura K, Takekawa S, Niwa K, Yajima Y, Iyi N, et al. J Cryst Growth 2001;211:230.
[6] Furukawa Y, Kitamura K, Takekawa S, Niwa K, Hatano H. Opt Lett 1998;23:1892.
[7] Zhang T, Wang B, Ling FR, Fang SQ, Xu YH. Mater Chem Phys 2004;83:350.
[8] Abdi F, Aillerie M, Bourson P, Fontana MD, Polgar K. J Appl Phys 1998;84:2251.
[9] Sun DL, Hang Y, Zhang LH. J Synth Cryst 2002;31:314.
[10] Furukawa Y, Sato M, Nitanda F, Ito K. J Cryst Growth 1990;99:832.
[11] Li MH, Xu YH, Wang R, Zhen XH, Zhao CZ. Cryst Res Technol 2001;36:191.
[12] Xu J, Zhang G, Liu S, Liu J, Men L. Appl Phys Lett 1994;64:2332.
[13] Zhang G, Liu S, Tian G, Xu J, Sun Q, Zhang G. Appl Opt 1997;36:1815.
[14] Zhang GQ, Zhang GY, Liu SM, Xu JJ, Sun Q. J Appl Phys 1998;83:4392.
[15] Zhong G, Jian J, Wu Z. In: Proceedings of the 11th International Conference on Quantum Electronics, IEEE, New York, 1990. p. 631.
[16] Volk TR, Pryalkin VI, Rubinina NM. Opt Lett 1990;15:996.
[17] Volk TR, Rubinina NM. Ferroelect Lett 1992;14:37.
[18] Kong Y, Wen J, Wang HF. Appl Phys Lett 1995;66:280.
[19] Yamanoto JK, Kitamura K, Iyi N, Kimura S, Furukawa Y, Sato M. Appl Phys Lett 1992;61:2156.
[20] Zhang Y, Xu YH, Li MH, Zhao YQ. J Cryst Growth 2001;233:537.
[21] Polgár K, Péter Á, Kovács L, Corradi G, Szaller Zs. J Cryst Growth 1997;177:211.
[22] Polgár K, Péter Á, Földvári I. Opt Mater 2002;19:7.
[23] Bordui PF, Norwood RG, Jundt DH, Fejer MM. J Appl Phys 1992;71:875.
[24] Zhen XH, Zhao LC, Xu YH. Appl Phys B 2003;76:655.
[25] Volk T, Rubinina N, Wöhlecke M. J Opt Soc Am B 1994;11:1681.
[26] Donnerberg H, Tomlison SM, Catlow CRA, Schirmer OF. Phys Rev B 1989;40:11909.